AIP Journal of Applied Physics

Amorphous silicon passivated contacts for diffused junction silicon solar cells

J. Bullock, D. Yan, Y. Wan, A. Cuevas, B. Demaurex, A. Hessler-Wyser, and S. De Wolf

Citation: Journal of Applied Physics **115**, 163703 (2014); doi: 10.1063/1.4872262
View online: http://dx.doi.org/10.1063/1.4872262
View Table of Contents: http://scitation.aip.org/content/aip/journal/jap/115/16?ver=pdfcov
Published by the AIP Publishing

Articles you may be interested in

Compositional study of defects in microcrystalline silicon solar cells using spectral decomposition in the scanning transmission electron microscope
Appl. Phys. Lett. **102**, 133902 (2013); 10.1063/1.4800569

Influence of back contact roughness on light trapping and plasmonic losses of randomly textured amorphous silicon thin film solar cells
Appl. Phys. Lett. **102**, 083501 (2013); 10.1063/1.4793415

Fabrication of solution-processed hydrogenated amorphous silicon single-junction solar cells
Appl. Phys. Lett. **100**, 253908 (2012); 10.1063/1.4730614

Photocurrent increase in n - i - p thin film silicon solar cells by guided mode excitation via grating coupler
Appl. Phys. Lett. **96**, 213508 (2010); 10.1063/1.3435481

Surface passivation properties of boron-doped plasma-enhanced chemical vapor deposited hydrogenated amorphous silicon films on p -type crystalline Si substrates
Appl. Phys. Lett. **88**, 022104 (2006); 10.1063/1.2164902

[This article is copyrighted as indicated in the article. Reuse of AIP content is subject to the terms at: http://scitation.aip.org/termsconditions. Downloaded to] IP: 128.178.170.160 On: Fri, 07 Nov 2014 14:04:01

JOURNAL OF APPLIED PHYSICS **115**, 163703 (2014)

Amorphous silicon passivated contacts for diffused junction silicon solar cells

J. Bullock,[1,a)] D. Yan,[1] Y. Wan,[1] A. Cuevas,[1] B. Demaurex,[2] A. Hessler-Wyser,[2] and S. De Wolf[2]
[1]*Research School of Engineering, The Australian National University, Canberra, ACT 0200, Australia*
[2]*École Polytechnique Fédérale de Lausanne (EPFL), Institute of micro engineering (IMT), Photovoltaics and Thin Film Electronic Laboratory, Maladière 71, CH-200 Neuchâtel, Switzerland*

(Received 7 February 2014; accepted 11 April 2014; published online 24 April 2014)

Carrier recombination at the metal contacts is a major obstacle in the development of high-performance crystalline silicon homojunction solar cells. To address this issue, we insert thin intrinsic hydrogenated amorphous silicon [*a*-Si:H(*i*)] passivating films between the dopant-diffused silicon surface and aluminum contacts. We find that with increasing *a*-Si:H(*i*) interlayer thickness (from 0 to 16 nm) the recombination loss at metal-contacted phosphorus (n^+) and boron (p^+) diffused surfaces decreases by factors of ∼25 and ∼10, respectively. Conversely, the contact resistivity increases in both cases before saturating to still acceptable values of ∼ 50 mΩ cm^2 for n^+ and ∼100 mΩ cm^2 for p^+ surfaces. Carrier transport towards the contacts likely occurs by a combination of carrier tunneling and aluminum spiking through the *a*-Si:H(*i*) layer, as supported by scanning transmission electron microscopy–energy dispersive x-ray maps. We explain the superior contact selectivity obtained on n^+ surfaces by more favorable band offsets and capture cross section ratios of recombination centers at the *c*-Si/*a*-Si:H(*i*) interface. © *2014 AIP Publishing LLC*. [http://dx.doi.org/10.1063/1.4872262]

I. INTRODUCTION

High-efficiency homojunction silicon solar cells have reached a point in their development where carrier recombination at the metal-silicon contact has a significant and sometimes limiting effect on device performance. This is commonly evidenced by relatively low open-circuit voltage values, compared to, e.g., silicon-heterojunction (SHJ) solar cells, which do not apply metal directly to the crystalline silicon absorber.[1] This issue has spawned much research in the area of "contact passivation".[2–6]

On homojunction solar cells, contact passivation can be achieved by inserting a thin dielectric interlayer that physically displaces the metal from the crystalline silicon (*c*-Si) surface, in a metal–insulator–semiconductor (MIS) type configuration. This was initially applied at the device level using thermally grown SiO_2[2] and has more recently been trialed with atomic-layer-deposited Al_2O_3.[3] A modification of this approach is to replace the metal with heavily doped poly-silicon, or another conductive over-layer, which further improves the selectivity of the contact.[4,5] The efficacy of the MIS type contact scheme is reliant on film-thickness control at the monolayer-level, as a delicate trade-off between increasing contact resistance and decreasing interface recombination exists for both SiO_2 and Al_2O_3.[6] This is directly linked to the wide bandgap of the dielectrics trialed so far and presents a significant challenge for industrial implementation.

In this article, we propose the use of intrinsic hydrogenated amorphous silicon (*a*-Si:H(*i*)) as an alternative interlayer. This film has a lower bandgap than the previously mentioned dielectrics and hence may offer a weaker dependence of the contact resistivity on thickness. In addition, such films have silicon surface passivation properties on par with the best dielectrics. Both properties are already successfully exploited in the intrinsic buffer layers used in SHJ solar cells, yielding conversion efficiencies as high as 24.7%, to date.[7] As with most device structures containing *a*-Si:H(*i*), a strong restriction on the temperature of processing is required, as annealing may irreversibly deteriorate the microstructure and passivation properties of the films. The presence of doped over-layers and metals may place even greater restrictions on the thermal processing of the device. Doped over-layers can lower the defect-creation energy,[8] while many metals induce crystallisation and protrude through *a*-Si:H(*i*) at low temperatures.[9] In particular, the application of aluminum directly to *a*-Si:H(*i*), as is the case in this study, remains a contentious combination in the context of solar cells.[9–11]

The applicability of the *a*-Si:H(*i*) contact interlayer is trialed here on both boron (p^+) and phosphorus (n^+) diffused surfaces, usually employed as the hole and electron collecting regions in traditional silicon solar cells. A simplified representation of the equilibrium energy band diagram of the structures tested in this study is provided in Figure 1. Identical *a*-Si:H(*i*)/Al stacks are used for the boron and phosphorus contacts. The contact resistivity ρ_c and the recombination parameter of the metal-contacted dopant diffusions J_{0c} are taken as the two metrics of importance, where low values are desired for both. The results are examined in terms of increasing *a*-Si:H(*i*) interlayer thickness in an effort to find an optimum value. Scanning transmission electron microscopy (STEM) is used in conjunction with energy dispersive x-ray (EDX) mapping to investigate the nature of the interfaces and the conduction mechanisms.

[a)]Electronic mail: james.bullock@anu.edu.au

 © 2014 AIP Publishing LLC

[This article is copyrighted as indicated in the article. Reuse of AIP content is subject to the terms at: http://scitation.aip.org/termsconditions. Downloaded to] IP: 128.178.170.160 On: Fri, 07 Nov 2014 14:04:01

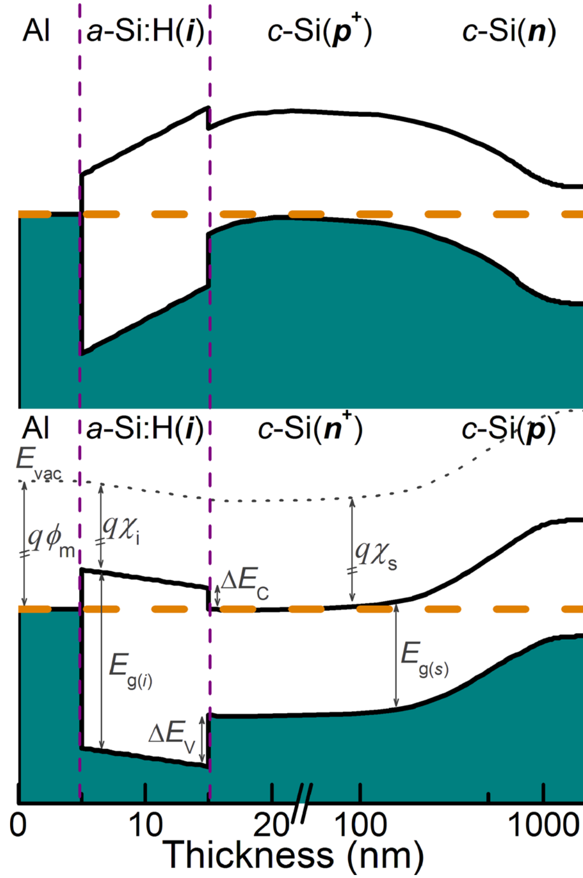

FIG. 1. Simplified equilibrium energy band diagrams representative of the hole-selective (top figure) and electron-selective (bottom figure) structures investigated in this study, as simulated by Automat for Simulation of Hetrostructures (AFORS-HET).[12] Assumed values; Al work function ϕ_m (4.23 V), *a*-Si:H(*i*) electron affinity χ_i (3.8 V), *c*-Si electron affinity χ_s (4.05 V), *a*-Si:H(*i*) mobility band gap $E_{g(i)}$ (1.82 eV),[13] *c*-Si band gap $E_{g(s)}$ (1.12 eV), *a*-Si:H(*i*)/ *c*-Si valence band offset ΔE_V (0.45 eV), and *a*-Si:H(*i*)/*c*-Si conduction band offset ΔE_C (0.25 eV).[13]

II. EXPERIMENTAL METHODS

A. Sample preparation

Symmetrical test structures were prepared using high resistivity (>100 Ω cm), (100), "Float-zone", p and n-type silicon wafers. The high resistivity of these wafers simplifies the extraction of recombination parameters. They were subjected to a 2 min alkaline saw damage etch and their surfaces were chemically polished in a HF:HNO_3 solution. Following a standard RCA clean, the samples were diffused symmetrically in dedicated clean quartz furnaces using a $POCl_3$ source (on p-type wafers) or a BBr_3 source (on n-type wafers) so that in all cases the doping of the substrate and diffusion were of opposite polarity. Two diffusion recipes were used for each source; the phosphorus diffused samples underwent a further short etch-back process to reduce the surface dopant concentration. The resultant final attributes of the four diffusion sets are given in Table I.

Following another RCA clean, each of the diffusion sets was deposited symmetrically with thicknesses of *a*-Si:H(*i*), in the range of 1–16 nm, using an Oxford PlasmaLab 100 plasma-enhanced-chemical-vapor-deposition (PECVD) instrument. The wafer temperature during deposition was estimated to be ∼350 °C, which is uncharacteristically high for *a*-Si:H(*i*). At this temperature epitaxial growth of silicon is expected leading to poor quality surface passivation.[14] Despite this, we found this temperature to provide optimum passivation in the as-deposited state, suggesting that no epitaxial growth has occurred. At this point samples were further separated into two groups to be developed into symmetrical lifetime structures (for assessing the contact recombination) or transfer-length-method (TLM) structures (for assessing the contact resistivity).

TABLE I. Dopant diffusion characteristics and recombination parameters of the four diffusion sets. R_{sh}, sheet resistance; N_{surf}, surface concentration; J_{0_metal}, recombination parameter of metallised diffusion region; J_{0_pass}, recombination parameter of passivated diffusion region.

Source	R_{sh} (Ω/□)	N_{surf} (cm^{-3})	J_{0_metal} (fA/cm^2)	J_{0_pass} (fA/cm^2)
$POCl_3$	85 ± 5	$4(\pm 1) \times 10^{19}$	1050 ± 200	55 ± 5
$POCl_3$	110 ± 10	$3(\pm 1) \times 10^{19}$	1200 ± 200	41 ± 5
BBr_3	110 ± 10	$1(\pm 1) \times 10^{19}$	1370 ± 200	27 ± 5
BBr_3	170 ± 15	$1(\pm 1) \times 10^{19}$	1900 ± 200	15 ± 5

The lifetime test structures were coated with aluminum on both sides in a vacuum thermal deposition system to a thickness of <15 nm, which is sufficiently thin to allow light through for photoconductance decay (PCD) measurements to be taken. PCD measurements were performed using a Sinton WCT 120 instrument under both transient and quasi-steady-state modes. The recombination current parameters J_{0c} of the *c*-Si(n^+)/*a*-Si:H(*i*)/Al and *c*-Si(p^+)/*a*-Si:H(*i*)/Al stacks were extracted from the PCD data using an intrinsic carrier concentration of $n_i = 8.95 \times 10^9\ cm^{-3}$ (at 25 °C) and the well-known Kane and Swanson method.[15] The parameter J_{0c} is a representation of the total minority carrier recombination occurring in the sub-surface diffusion region (predominantly Auger recombination) and at the diffused surface (predominantly Shockley–Read–Hall recombination).

TLM structures were created by evaporating ∼1 μm of aluminum onto the *a*-Si:H(*i*) passivated p^+ and n^+ surfaces. Contact pads were photolithograpically defined and isolated using an acidic aluminum etch. A 15 min 110 °C anneal is required to hard-bake the photoresist before the acidic etching. Current–voltage measurements were performed (Keithley 2425 Source Meter) at ∼297 K on pad spacings in the range of 10–300 μm and ρ_c was extracted as per the description given in Ref. 16. As a point of clarification, in this study, the measured ρ_c reflects the average of both bias directions (implicit in TLM), where the resistivity in each direction comprises the resistance through the *a*-Si:H(*i*) as well as across the *a*-Si:H(*i*)/Al and *c*-Si/ *a*-Si:H(*i*) interfaces. It was also assumed that the parallel sheet conductance between pads through the *a*-Si:H(*i*) layer is negligible.

B. Reference recombination parameters

Included in Table I as a reference are the measured recombination parameters for diffusions covered by either only a metal film (J_{0_metal}) or a high-quality passivation film without a metal over-layer (J_{0_pass}). A thin aluminum layer (<15 nm) is used to create the directly metallized surface.

[This article is copyrighted as indicated in the article. Reuse of AIP content is subject to the terms at: http://scitation.aip.org/termsconditions. Downloaded to] IP: 128.178.170.160 On: Fri, 07 Nov 2014 14:04:01

The high-quality passivation films consisted of ~20 nm of plasma-assisted atomic-layer-deposited (PA-ALD) Al_2O_3 (Beneq TFS, 200 ALD instrument) on the boron-diffused surfaces and ~75 nm of PECVD a-SiN_x:H (Roth & Rau AK 400) on the phosphorus surfaces. The large positive fixed charge density in a-SiN_x:H and negative fixed-charge density in Al_2O_3 reduce the minority carrier concentrations at the n^+ and p^+ c-Si surfaces, respectively, which results in very low surface recombination even for moderate interface state densities. In comparison, a-Si:H(i) films exhibit no strong fixed charge, but achieve a very effective reduction of the density of interface states ($<10^9\,cm^{-3}$),[17] making them ideal candidates for the passivation of both n^+ and p^+ surfaces.

Given the high quality of passivation obtained by the Al_2O_3 and a-SiN_x:H layers, the J_{0_pass} values provided in Table I can be viewed as an approximate upper-limit for the recombination occurring in the subsurface diffused regions, which is mostly due to the Auger process.

C. Photoluminescence analysis

Inherent in the analysis to follow is the assumption that lifetime test structures (aluminum thickness <15 nm) produce the same carrier recombination as actual (passivated) metal contacts, such as those present in the TLM test structures (aluminum thickness of ~1 μm). To verify this assumption, a photoluminescence (PL) analysis (BT Imaging LIS-R1) was performed on two symmetrically diffused (n^+) and passivated samples with ~15 and ~30 nm of a-Si:H(i). On the rear side of the two samples, half of the area was evaporated with thin (<15 nm) and the other half with thick (1 μm) aluminum. Both samples were annealed at 110 °C for 15 min before imaging. PL images were taken (rear side down) using a set illumination intensity with and without a short-pass filter of 1000 nm. The images taken without the filter are representative of a broader wavelength range and include longer wavelengths, which have a penetration depth greater than the thickness of the wafer. It is therefore expected that the region with the thicker aluminum (greater rear side reflection) will appear brighter, provided differences in carrier recombination are not significant. The image taken with the filter in place includes only wavelengths with penetration lengths significantly less than the thickness of the wafer—hence if there are no differences in carrier recombination, there should be no visible difference between the thick and thin metal regions. Figure 2 shows the two sets of PL images taken of the same region with and without a short-pass filter, where brighter colours represent a higher PL signal and thus longer effective carrier lifetime. In all cases, the above behavior is followed, demonstrating that there are no major differences in carrier recombination between the thin and thick metallisation schemes.

D. Ellipsometry and transmission electron microscopy measurements

During all a-Si:H(i) depositions, a single side, mechanically polished wafer was included to monitor film thickness. Reflectance spectra of these samples were measured using a

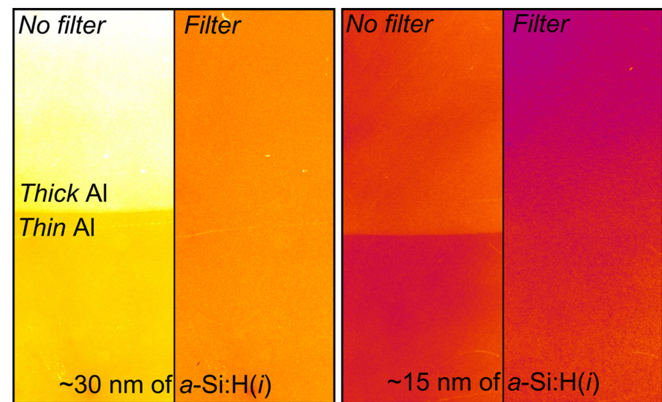

FIG. 2. PL images of samples with ~30 and ~15 nm of a-Si:H(i) taken with and without a short-pass filter. Without a filter images reveal different rear reflection. With a filter, the influence of rear reflection is removed, and the images indicate similar surface recombination for the two thicknesses of aluminum. All four images are scaled individually to highlight contrasts across the imaged region.

J.A Woolam M-2000 variable angle ellipsometer and thicknesses were obtained using a Tauc-Lorentz material model.[18]

STEM samples were also prepared from single-side mechanically polished wafers. These were deposited with ~28 nm of a-Si:H(i) and ~1 μm of aluminum following which they were annealed at 110 °C for 15 min. TEM lamellae were prepared by mechanical polishing in a wedge-shape configuration with a Tripod polisher then ion milling with Ar ions (Gatan PIPS). The preparation sequence before imaging required a temperature step at ~130 °C for over 30 min. An FEI Tecnai Osiris instrument was used to take bright field (BF) STEM micrographs and high sensitivity EDX maps of aluminum, silicon and oxygen.

III. RESULTS AND DISCUSSION

A. Interface passivation

The recombination current parameter J_{0c} as a function of a-Si:H(i) thickness is shown for the two phosphorus diffusions in Figure 3(a) and for the two boron diffusions in Figure 3(b). The quality of the as-deposited surface passivation on the phosphorus diffusion improves dramatically with a-Si:H(i) thickness and appears to saturate in the 6–8 nm range, consistent with open circuit voltage V_{oc} trends for SHJ solar cells reported in the literature.[19] Beyond these thicknesses excellent passivation is achieved, producing recombination parameters even lower (by about 10 fA/cm^2) than the PECVD a-SiN_x:H controls listed in Table I, inferring that this value is a more appropriate upper-limit representation of recombination within the bulk of the phosphorus diffusion. An alike sample (not shown) deposited with ~30 nm of a-Si:H(i) produces an identical J_{0c} to that at 10 nm confirming that the passivation is saturated. Whilst an expected slight difference in the magnitude of recombination between the 85 and 110 Ω/□ n^+ diffusions is seen, the general behaviour of both n^+ diffusions can be well represented by a single trendline, adding to the confidence in the measured results.

Following metallisation, a significant increase in J_{0c} was observed for a-Si:H(i) thicknesses below 10 nm. The spread

[This article is copyrighted as indicated in the article. Reuse of AIP content is subject to the terms at: http://scitation.aip.org/termsconditions. Downloaded to] IP: 128.178.170.160 On: Fri, 07 Nov 2014 14:04:01

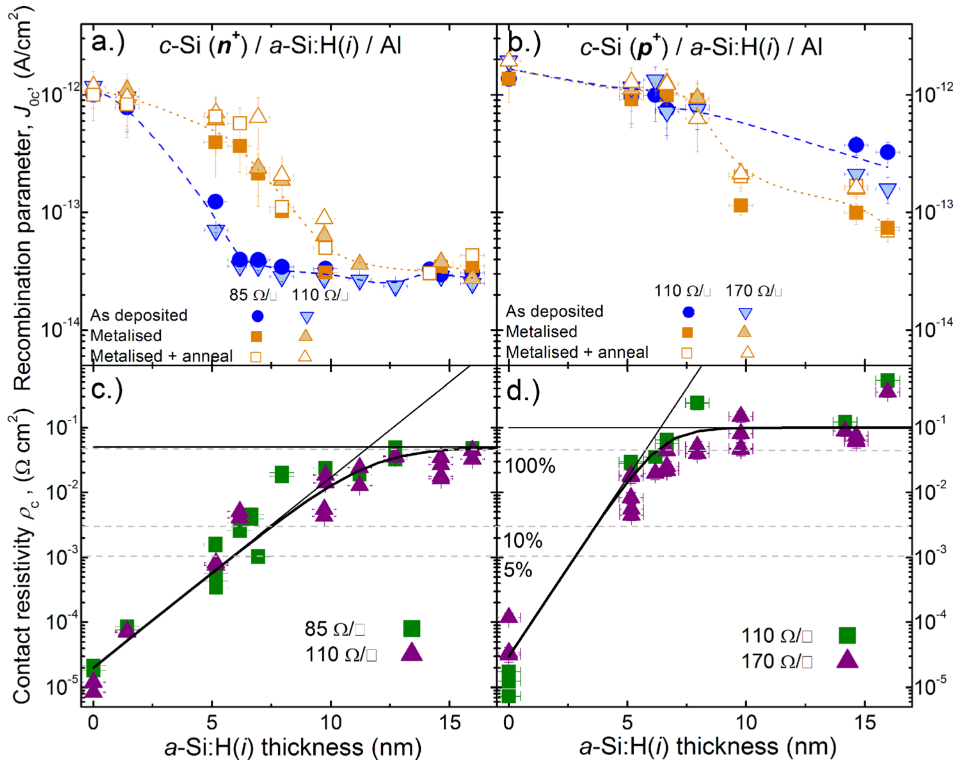

FIG. 3. Contact recombination parameter J_{0c} for (a) phosphorus and (b) boron diffused surfaces and contact resistivity ρ_c for (c) phosphorus and (d) boron diffused surfaces as a function of *a*-Si:H(*i*) thickness. The dotted blue and orange lines provide a guide to the eye for the as-deposited (blue) and metallised (orange) results. The dashed lines represent reference values for contacts with a total contact resistance R_c of ~0.05 Ω cm^2, having areas of respectively 5, 10, and 100% of the wafer surface (see Sec. III E). Error bars are based on the measured spread in data or the estimated error of the measurement (whichever was largest).

in measured data and uncertainty in determining J_{0c} values also greatly increase in this region, as indicated by the large error bars in Figure 3. Whilst there were some small increases in recombination evident for samples with *a*-Si:H(*i*) thicknesses above 10 nm, the J_{0c} values remained close to the corresponding pre-metallisation values. To provide a direct comparison to the TLM structures some of the metallised n$^+$ symmetrical lifetime samples were annealed for 15 min at 110 °C as shown in Figure 3(a). It can be seen that whilst some additional increase in recombination is caused by the anneal, excellent passivation is still achievable for *a*-Si:H(*i*) thicknesses above 10 nm.

There are four foreseeable causes for the increase in J_{0c} when a metal overlayer is present: (i) penetration of the *c*-Si minority carrier wavefunctions through the *a*-Si:H(*i*) film to the *a*-Si:H(*i*)/Al interface, where rapid recombination is possible;[20] (ii) the onset of depletion conditions at the heavily diffused *c*-Si surfaces again caused by the aluminum work function, resulting in a change the recombination statistics at the *c*-Si surface;[21,22] (iii) a lowering of the Fermi-level within the *a*-Si:H(*i*) film by the aluminum work function, potentially leading to a lower defect formation enthalpy in the *a*-Si:H(*i*) film;[8] or (iv) partial protrusion of the aluminum through the *a*-Si:H(*i*), possibly making contact with the *c*-Si surface.[9] A low temperature interaction between aluminum and *a*-Si:H(*i*) has been outlined in many previous studies,[9–11] some of which suggest that conditions experienced during aluminum vacuum depositions are sufficient to initiate this interaction. Below we confirm that indeed some aluminum spiking has occurred.

The boron diffused samples in Figure 3(b) show a more gradual improvement in as-deposited passivation with *a*-Si:H(*i*) thickness and do not achieve as good a level of passivation as the controls listed in Table I. Under these deposition conditions, an additional sample (not shown) with an *a*-Si:H(*i*) thickness of ~30 nm produced a recombination parameter of ~70 fA/cm^2 for both p$^+$ diffusions, considerably lower than the 15 nm samples but still well above the controls listed in Table I. Avoiding a postdeposition anneal was a central premise of this work; hence, the deposition conditions were chosen to provide the highest as-deposited *a*-Si:H(*i*) passivation. However, in a separate study, we have found that the passivation provided by thicker *a*-Si:H(*i*) films (>12 nm) improved upon annealing, presumably due to a reduction in D_{it} from additional hydrogenation. Therefore, lower J_{0c} may be attainable if a re-optimisation of the *a*-Si:H(*i*) films based on annealing was performed. Following metallisation, J_{0c} improved for *a*-Si:H(*i*) thicknesses greater than 10 nm, possibly due to a small annealing effect during the thermal evaporation of aluminum. Further annealing at 110 °C for 15 min resulted in no further improvement, rather in increases in J_{0c}. The higher surface recombination evident on the p$^+$ surface relative to the n$^+$ is potentially due to *c*-Si/*a*-Si:H(*i*) interface defects exhibiting an electron to hole capture cross section area ratio (σ_n/σ_p) greater than unity.[23]

B. Contact resistivity

The specific contact resistivity ρ_c for the phosphorus and boron diffusions as a function of *a*-Si:H(*i*) thickness are provided in Figures 3(c) and 3(d), respectively. For the phosphorus diffusion, the dependence of ρ_c on the thickness of the *a*-Si:H(*i*) interlayer can be separated into two regimes; an approximately exponential increase for the first 10 nm followed by a plateauing of ρ_c. This behavior appears to be largely independent of the underlying doping, as both the 85 and 100 Ω/□ diffusions yield similar trends.

Both boron-diffused surfaces exhibit a steeper initial increase in ρ_c and plateau at a higher value relative to the n$^+$

[This article is copyrighted as indicated in the article. Reuse of AIP content is subject to the terms at: http://scitation.aip.org/termsconditions. Downloaded to] IP: 128.178.170.160 On: Fri, 07 Nov 2014 14:04:01

surfaces. A potential explanation for the higher ρ_c on p^+ surfaces may be found in the well-known asymmetry between the conduction and valence band offsets at the *c*-Si/*a*-Si:H(*i*) interface.[13] These offsets contribute to effective barriers for electron and hole transport at the *c*-Si surface, as depicted in Figure 1. A significantly smaller conduction band offset, as compared to the valence band offset has been reported by many studies at this interface which suggest a greater conductivity across the interface for electrons (in n^+ silicon) than holes (in p^+).[13] Studies of window layers in SHJ solar cells equally pointed out that the valence-band offset may hinder efficient hole transport through passivation stacks.[24] An additional possible explanation is the formation of a large energy barrier at the p^+ *c*-Si surface caused by the low work function of aluminum.[21] An alike barrier forming on the n^+ surface would be smaller owing to a higher *c*-Si surface concentration (compared to the p^+ contact) and a smaller difference between the n^+ *c*-Si Fermi energy and the Al work function.

C. Structural composition of the layers

STEM-EDX analysis of the contact stack, presented in Figure 4, was taken to better understand the interfacial uniformity and conduction mechanisms. Figure 4(a) shows the bright field STEM image of a *c*-Si/*a*-Si:H(*i*)/Al (1 μm) structure. Note that the *a*-Si:H(*i*) film was made intentionally thicker ($\sim$28 nm) than the lifetime and TLM samples for characterisation purposes. Uniform surfaces are seen at both the *c*-Si/*a*-Si:H(*i*) and the *a*-Si:H(*i*)/polycrystalline Al interfaces. As opposed to the polycrystalline Al layer, an absence of diffraction contrast in the *a*-Si:H(*i*) layers suggests that it remains in an amorphous state. The dark line at the *c*-Si/*a*-Si:H(*i*) interface is believed to be a measurement artifact rather than an interfacial species. Figures 4(b)–4(d) provide 2D EDX maps of the local O, Al and Si concentration through the entire depth of the sample (>100 nm), for the same region as shown in Figure 4(a). Figure 4(b) reveals that both interfaces host a thin unintentional oxide layer, the thicker of which is between Al and *a*-Si:H(*i*) films. The thin oxide at the *c*-Si/*a*-Si:H(*i*) interface may assist in maintaining amorphous growth during the high-temperature deposition, similar to the use of silicon-oxide deposition to prevent epitaxial film growth.[25] Local hemispherical protrusions can be seen originating from the aluminum layer in Figure 4(c) (which maps the Al concentration), suggesting partial spiking of the Al through the *a*-Si:H(*i*) film, which is supported by corresponding regions of lower silicon concentration in Figure 4(d). The higher temperature procedure (130 °C) used for the STEM samples designate the obtained images as upper-limit representations of the aluminum spiking occurring in the TLM and lifetime samples.

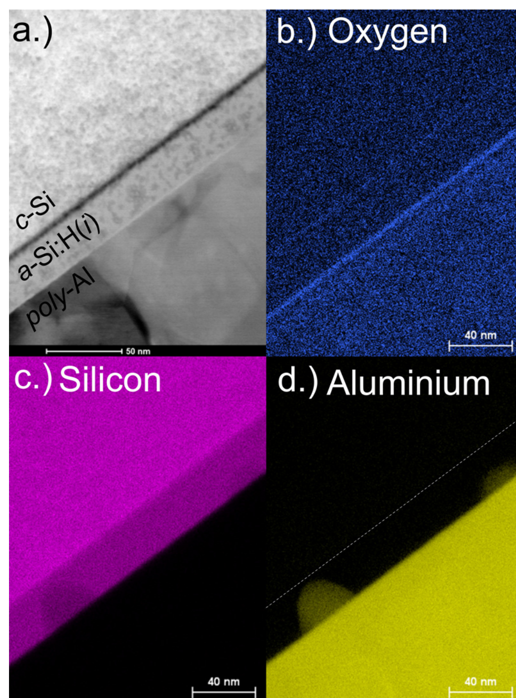

FIG. 4. (a) Bright field STEM image of the *c*-Si/*a*-Si:H(*i*)/Al stack. EDX maps of the same region for (b) oxygen, (c) silicon, and (d) aluminum. The white dashed line in (d) represents the position of the *c*-Si/*a*-Si:H(*i*) interface.

D. Conduction mechanisms

A lower limit protrusion depth of $\sim$20 nm can be estimated from the cross sectional images, implying that direct contact is most likely made to the *c*-Si surface for all thicknesses of *a*-Si:H(*i*) tested in the present study. These findings suggest that some conduction is achieved through a nanoscale partial contact structure. However, this conduction mechanism is unlikely to fully explain the thickness dependent ρ_c behavior observed for both the n^+ and p^+ surfaces. Instead, the results for ρ_c against *a*-Si:H(*i*) thickness suggest that the total conduction is the consequence of both direct contact through the aluminum protrusions, which has no strong dependence with interlayer thickness in the range of 0–15 nm, and a second parallel conduction mechanism with an exponential dependence on *a*-Si:H(*i*) thickness as illustrated in Figure 3. A candidate for the second mechanism, supported also in the literature,[26] is quantum-mechanical tunneling through the *a*-Si:H(*i*) layer; other conduction mechanisms, such as thermionic emission could not easily explain this trend. Starting from very thin *a*-Si:H(*i*) interlayers, a tunneling conduction mechanism could initially dominate the total conduction. The conductivity through this pathway would be expected to exponentially decrease (resistivity would exponentially increase) with increasing *a*-Si:H(*i*) interlayer thickness. At thicknesses of approximately 8 nm, the tunneling current becomes smaller than the direct conduction pathway through the aluminum protrusions, which dominates at thicknesses above this point, explaining the plateauing of ρ_c. It is expected that for *a*-Si:H(*i*) thicknesses greater than the protrusion depth (outside the measured range) the resistivity would be again higher.

In an effort to quantify the above suggestion of two parallel conduction pathways, the ρ_c trends in Figures 3(c) and 3(d) were each fitted with the inverse sum of two functions. One is a constant independent of thickness $\rho_{c1}(t) = c$, representative of spiking conduction; and the other function is

[This article is copyrighted as indicated in the article. Reuse of AIP content is subject to the terms at: http://scitation.aip.org/termsconditions. Downloaded to] IP: 128.178.170.160 On: Fri, 07 Nov 2014 14:04:01

exponentially dependent on the thickness $\rho_{c2}(t) = a\ \exp(bt)$, representative of tunneling conduction. The second function $\rho_{c2}(t)$, can be compared to an approximate analytical expression for the inverse of the tunneling transmission coefficient T through a rectangular potential barrier given by[27]

$$\frac{1}{T(t)} = \exp\left(2t\sqrt{\frac{2m^*_{(e,h)}q\Phi_{eff(C,V)}}{\hbar^2}}\right) \propto \rho_c(t), \qquad (1)$$

where ρ_c is inversely proportional to the tunneling transmission coefficient T. $m^*_{(e,h)}$ is the tunneling effective electron or hole mass within the *a*-Si:H(*i*) layer, $\hbar$ is the reduced Plank constant, q is the elementary charge, and $\Phi_{eff(C,V)}$ is the effective barrier presented to conduction band electrons or valence band holes.

By equating the exponents of the modelled contact resistivity $\rho_{c2}(t)$ and Eq. (1), it is possible to check if, as stated in Sec. III B, the differences in slope observed for the $\rho_c(t)$ trends of the n^+ and p^+ contacts can be accounted for by differences in valence and conduction band offsets. The ratio of the fitted constants b of the p^+ and n^+ contact structures can be related to terms in Eq. (1) by

$$\left(\frac{b^2_{p+}}{b^2_{n+}} = 3.5\right) \approx \frac{m^*_h\Phi_{eff(V)}}{m^*_e\Phi_{eff(C)}}, \qquad (2)$$

which is measured to be 3.5 in the present work. From trusted values in the literature presented in Figure 1, a $\Phi_{eff(C)}$ value of $\sim$0.34 eV is calculated from the average height of the *a*-Si:H(*i*) conduction band above the *c*-Si conduction band. A similar analysis can be performed by comparison of the *a*-Si:H(*i*) and *c*-Si valence bands in Figure 1 to obtain a $\Phi_{eff(V)}$ value of $\sim$0.92 eV. The values and validity of using electron and hole effective masses in *a*-Si:H(*i*) remain a contentious point;[28] however, if the assumption is made that the electron and hole effective masses are of a similar magnitude, then the calculated ratio in Eq. (2) is $\sim$2.7, comparing reasonably well with the measured value of 3.5.

Although the measured exponential dependence of resistivity on thickness strongly suggest that tunneling through the *a*-Si:H(*i*) is a contributing mechanism to conduction, further studies are required to unequivocally confirm its role, given the complex nature of the contact and the aluminum—*a*-Si:H(*i*) interaction and the uncertainties in the band offsets and effective masses.

E. Consequences for solar cell performance

The above results demonstrate that whilst complete isolation of the aluminum and *c*-Si was not possible under these processing conditions, excellent contact characteristics were still achieved, particularly on the n^+ surface. Included in Figures 3(c) and 3(d) as an approximate guide are lines (horizontal dashed lines) indicating appropriate ρ_c values for 5%, 10%, and 100% contact area, chosen in line with a total contact resistance R_c of 0.05 Ω cm^2. For the phosphorus diffused contacts in Figure 3(c) it can be seen that the ρ_c limit for both the 5% and 10% contact fractions is exceeded in the 5–7 nm range where J_{0c} values still exhibit high recombination of $\sim$500 fA/cm^2. This situation can be improved by choosing full-area rear contacts, for which *a*-Si:H(*i*) thicknesses up to 15 nm are acceptable in terms of ρ_c. In this region J_{0c} values of $\sim$40 fA/cm^2 are consistently attained for both 85 and 110 $\Omega/\square$ n^+ diffusions. Similarly, the boron diffused contacts in Figure 3(d) suggest that the optimum configuration is again a full area contact; however, in this instance, J_{0c} values in the 200–700 fA/cm^2 are to be expected—far higher than those on n^+ surfaces.

For an estimation of the V_{oc} gain attained by applying the n^+ contact to a solar cell, we introduce a comparison full-area deep phosphorus back surface region, which is known to have an optimum recombination parameter of $\sim$300 fA/cm^2. Using the optimum post-metallisation J_{0c} value of $\sim$40 fA/cm^2 (with $\sim$14 nm of *a*-Si:H(*i*)) found in this study, an upper-limit V_{oc} gain of $\sim$50 mV is calculated over an optimized full-area heavy phosphorus diffusion, using the method given in Ref 6. A similar analysis for the p^+ surface provides less impressive results.

In summary, the results detailed in this paper present a simple modification to conventional homojunction solar cells which attains a high level of contact passivation. However, the sensitivity of the contact characteristics to temperature presents a technological challenge in ensuring low temperature back-end processing. Values in the literature suggest severe increases in recombination would result from temperatures in the vicinity of 180 °C,[9] and indeed, this study has shown that even temperatures as low as 110 °C will affect device performance. The use of other metals with a higher *a*-Si:H(*i*) interaction temperature or an overlying conductive buffer layer may prove beneficial in improving contact stability.

IV. CONCLUSION

As an alternative to an MIS contact, *a*-Si:H(*i*) was trialed as a passivating interlayer between heavily diffused phosphorus/boron surfaces and aluminum. The contact resistivity and contact recombination parameter were monitored as a function of *a*-Si:H(*i*) thickness in order to find the optimum. For both n^+ and p^+ diffusions a full area rear contact is found to be a suitable practical application of the passivated contact scheme developed in this paper. Superior majority carrier conductivity and surface passivation was found for the *c*-Si (n^+)/*a*-Si:H(*i*)/Al contact with a ρ_c of <0.05 Ω cm^2 and a J_{0c} of $\sim$40 fA/cm^2 for *a*-Si:H(*i*) thicknesses in the 12–15 nm range. These values translate to an upper-limit V_{oc} gain of $\sim$50 mV when compared to an optimised phosphorus back surface region. The *c*-Si (p^+)/*a*-Si:H(*i*)/Al contact failed to achieve as low resistivity and recombination results, a larger valence band offset and larger minority carrier capture cross section area of interface defects are possible causes for this difference. STEM EDX analysis reveals that small aluminum protrusions through the *a*-Si:H(*i*) layer may contact the *c*-Si directly, thus contributing to conduction. The exponential trend of contact resistivity on interlayer thickness suggests that quantum-mechanical tunneling is a second conduction mechanism, which dominates at lower *a*-Si:H(*i*) thicknesses.

[This article is copyrighted as indicated in the article. Reuse of AIP content is subject to the terms at: http://scitation.aip.org/termsconditions. Downloaded to] IP: 128.178.170.160 On: Fri, 07 Nov 2014 14:04:01

ACKNOWLEDGMENTS

The authors from the ANU acknowledge financial support by The Australian Solar Institute/Australian Renewable Energy Agency as well as access to equipment at the Australian National Fabrication Facility. The authors from EPFL thank the Axpo Naturstrom Fonds, the European Commission (FP7 project Hercules), the EuroTech Universities Alliance and the Swiss Commission for Technology and Innovation for their financial support. The authors thank Danièle Laub (EPFL) for the STEM sample preparation.

[1]S. De Wolf, A. Descoeudres, Z. C. Holman, and C. Ballif, Green **2**, 7 (2012).
[2]M. A. Green, A. W. Blakers, M. R. Willison, T. Szpitalak, E. M. Keller, E. Gauja, and P. J. Hart, in *Proceedings of the 15th IEEE Photovoltaic Specialist Conference, Kissimmee, USA, 1981*, p. 1405.
[3]D. Zielke, J. H. Petermann, F. Werner, B. Veith, R. Brendel, and J. Schmidt, Phys. Status Solidi RRL **5**, 298 (2011).
[4]P. Borden, L. Xu, B. McDougall, C. P. Chang, D. Pysch, P. Voisin, and S. W. Glunz, in *Proceeding of the 23th European Photovoltaic Specialist Conference, Valencia, Spain, 2008*, p. 1149.
[5]D. Garcia-Alonso, S. Smit, S. Bordihn, and W. M. M. Kessels, Semicond. Sci. Technol. **28**, 082002 (2013).
[6]J. Bullock, D. Yan, and A. Cuevas, Phys. Status Solidi RRL **7**, 946 (2013).
[7]M. Taguchi, A. Yano, S. Tohoda, K. Matsuyama, Y. Nakamura, T. Nishiwaki, K. Fujita, and E. Maruyama, IEEE J. Photovolt. **4**, 96 (2014).
[8]S. De Wolf and M. Kondo, J. Appl. Phys. **105**, 103707 (2009).
[9]H. Plagwitz, M. Nerdling, N. Ott, H. P. Strunk, and R. Brendal, Prog. Photovolt.: Res. Appl. **12**, 47 (2004).
[10]E. Schmich, E. van Kershaver, K. Fisher, and P. Basore, in *Proceedings of the 28th European Photovoltaic Specialist Conference, Paris, France, 2013*, p. 1271.
[11]T. F. Schulze, Ph.D. dissertation, Institut für Silizium-Photovoltaik E-I1, HZB, 2011.
[12]R. Stangl, M. Kriegel, and M. Schmidt, in *Proceeding of the 4th World Conference on Photovoltaic Energy Conversion, Hawaii, USA, 2006*, p. 1350–1353.
[13]T. F. Schulze, L. Korte, F. Ruske, and B. Rech, Phys. Rev. B. **83**, 165314 (2011).
[14]H. Fujiwara and M. Kondo, Appl. Phys. Lett. **90**, 013503 (2007).
[15]D. E. Kane and R. M. Swanson, in *Proceedings of the 18th IEEE Photovoltaic Specialist Conference, Las Vegas, USA, 1985*, p. 578–583.
[16]D. K. Schroder, *Semiconductor Material and Device Characterisation* (Wiley, Hoboken, 2006), p. 146.
[17]S. De Wolf, S. Olibet, and C. Ballif, Appl. Phys. Lett. **93**, 032101 (2008).
[18]G. E. Jellison, Jr. and F. A. Modine, Appl. Phys. Lett. **69**, 371 (1996).
[19]M. Tanaka, M. Taguchi, T. Matsuyama, T. Sawada, S. Tsuda, S. Nakano, H. Hanafusa, and Y. Kuwano, Jpn. J. Appl. Phys. **31**, 3518 (1992).
[20]S. De Wolf and M. Kondo, Appl. Phys. Lett. **91**, 112109 (2007).
[21]M. Bivour, C. Reichel, M. Hermle, and S. W. Glunz, Sol. Energ. Mat. Sol. Cells **106**, 11 (2012).
[22]D. Munoz, T. Desrues, P.-J. Ribeyron, A. Orpella, I. Martin, C. Voz, and R. Alubilla, Phys. Status Solidi C **7**, 1029 (2010).
[23]A. Descoeudres, Z. C. Holman, L. Barraud, S. Morel, S. De Wolf, and C. Ballif, IEEE J. Photovolt. **3**, 83 (2013).
[24]J. P. Seif, A. Descoeudres, M. Filipic, F. Smole, M. Topic, Z. C. Holman, S. De Wolf, and C. Ballif, J. Appl. Phys. **115**, 024502 (2014).
[25]H. Fujiwara, T. Kaneko, and M. Kondo, Appl. Phys. Lett. **91**, 133508 (2007).
[26]A. Kavevce and W. Metzger, J. Appl. Phys. **105**, 094507 (2009).
[27]S. M. Sze and K. K. Ng, *Physics of Semiconductor Devices* (Wiley-Interscience, 2007), p. 439.
[28]R. A. Street, *Hydrogenated Amorphous Silicon* (Cambridge Univ. Press, 2005), pp. 142–144.

[This article is copyrighted as indicated in the article. Reuse of AIP content is subject to the terms at: http://scitation.aip.org/termsconditions. Downloaded to] IP: 128.178.170.160 On: Fri, 07 Nov 2014 14:04:01